Journal of Chromatography, 119 (1976) 55–70

CHROM. 8930

INSTRUMENTAL CONTRIBUTIONS TO BAND BROADENING IN GAS CHROMATOGRAPHY

II. EXPERIMENTAL EVALUATION

STUART P. CRAM
Varian Aerograph, 2700 Mitchell Dr., Walnut Creek, Calif. 94598 (U.S.A.)
and
TOM H. GLENN, Jr.*
(Received November 7th, 1975)

SUMMARY

A precision gas chromatograph under the control of a digital data acquisition and control system is described which was designed to evaluate the band broadening contributions of a model system. The zeroth, first, and second moments of a non-sorbed peak are reported and the band-broadening contributions from the sample, mixing volumes, effective detector volume, and electronic time constants have been measured. Excellent agreement was found between the predicted values and the experimental results.

INTRODUCTION

With the development of high-precision gas chromatographic instrumentation and data acquisition systems, the contribution of the chromatographic instrumentation to the observed retention times and solute band broadening must be considered. This is of particular importance in studying the dynamics of on-column processes, in high-precision qualitative and quantitative analyses, and in systems where chemical processes do not limit the analytical characteristics of the separation or the analysis. Rigorous high-precision, experimental methods of detecting and measuring the instrumental contributions to retention and band broadening have not been previously developed. This work describes the measurement of the instrumental band broadening where there are several contributions present, and the separation of the effects of these contributions. A precision experimental system was designed and developed in which all of the experimental parameters were known or could be calculated. This system included all of the standard chromatographic components and was used to test a model that was designed to accurately represent the real system.

An example of the type of aberration that can be introduced by instrumental

* Author deceased.

effects was presented in Kieselbach's study[1] of the eddy diffusion term in the Van Deemter equation. He found that elimination of the mixing volumes removed the asymmetry of the air peak and reduced the velocity-independent term to a very small value. This was verified in a later paper[2] in which efforts were made to reduce the effects of the detector response speed and the mixing volumes of the apparatus. The improved resolution obtained in this manner allowed the experimental detection of a mass-transfer resistance effect which had not been measured before.

Knox and McLaren[3] were among the first to attempt to correct experimental data for the effects of instrumental contributions by the use of variances. Because the paper was concerned with the investigation of the coupling effect, there was no attempt to refine the estimation of the instrumental correction or to evaluate each component accurately. Other workers have derived equations for measuring and correcting an elution profile for mixing volume effects occurring after the column[4]. This theoretical approach was based on the solution of a differential equation for the concentration profile resulting from the mixing. The complexity of the method makes it relatively difficult to use in practice, especially when there are several factors to be measured.

The effects of mixing volumes, diffusion volumes, and the injection time were discussed by Guiochon[5,6]. The general treatment of the instrumental contributions to the band broadening was in terms of the dependence on the linear gas velocity. The individual expressions were obtained with a simple random-walk treatment, with the assumption that each of the contributions was independent of the other. The effects were presented in terms of their component plate heights which is not a desirable situation because this associates the instrumental contributions with a particular column.

Mathematical treatments of instrumental band broadening have been reported by Reilley *et al.*[7–9] which use discrete convolution methods and Laplace transforms to calculate the profile resulting from the operation of a column on several input profiles. Sternberg[10] has reviewed the theory of instrumental band-broadening effects and developed several examples to illustrate their effect on chromatographic measurements.

EXPERIMENTAL

Pneumatic system

The chromatographic equipment developed was designed so that all components of the instrument, pneumatic and electronic, were of well defined specifications so that the band-broadening contribution of each component could be reliably calculated or measured. The chromatographic system has previously been described[11]. The pneumatic system was modified for the work reported here to include a balanced pressure regulator (Model 41200649; Veriflo) followed in series by a single stage regulator (Model 41300451; Veriflo) which regulated and reduced the helium pressure to 100 p.s.i.g. The final stage of carrier gas regulation was a constant upstream flow controller (Model 42300079; Veriflo) with a fine metering valve.

The methane sample gas pressure was reduced by a two stage regulator (Model 8-350; Matheson) and the flow-rate was controlled by an extra fine metering valve (Model 343000184; Veriflo). Air and hydrogen were supplied to the flame detector

from cylinders equipped with balanced pressure regulators (Model 41200649; Veriflo). The hydrogen flow-rate was controlled by an extra fine metering valve (Model 43000184; Millaflow) and the air flow rate was controlled by a fine metering valve (Model 43000188; Millaflow). The air and hydrogen flow-rates were measured with a soap-film bubble meter and corrected for the vapor pressure of water. The flow-rate of the sample gas was too low to be measured accurately by this method, so it was calculated from the area of the peak and from the response factor for methane (0.251 C/mole)[12].

The sampling valve has been described in an earlier publication[11] but used a 3-mm separation between the helium inlet and the sample inlet tubes for this work. A 1.0 m × 0.660 mm I.D. capillary tube was used as the column in order to eliminate the complications of sorption in the column.

To determine the effect of the flame jet on the column outlet pressure, an ethylene glycol manometer was connected in place of the hydrogen supply. The helium flow-rate was adjusted so that the total flow-rate was 15 ml/sec. Under these conditions the pressure drop due to the flame jet was less than 2 mm of ethylene glycol. Therefore, the outlet pressure was assumed to be atmospheric.

The pressure drop across the column was measured with a mercury manometer on the column side of the sampling valve vent. The carrier gas flow-rate was measured by calibrating the capillary column as a flow meter and measuring the column inlet pressures. The flow-rate at the outlet of the capillary, F_0, was calculated from Poiseuille's equation

$$F_o = \frac{A \cdot k}{2 \eta L} \left(\frac{p_i^2 - p_o^2}{p_o} \right) \tag{1}$$

where A is the cross sectional area, k is a constant related to the geometry of the tube, η is the viscosity of the carrier gas, L is the length of the column, and p_i and p_0 are the inlet and outlet pressures, respectively. Due to the uncertainties in the carrier gas viscosity and the radius of the column, it was advantageous to collect all of the constants except the tube length into one constant and empirically evaluate that constant. Upon introducing a conversion factor so that the pressures may be expressed in cmHg, we have

$$F_0 = 1.333 \times 10^4 \cdot \left(\frac{K}{L} \right) \left(\frac{p_i^2 - p_o^2}{p_o} \right) \tag{2}$$

where K is the characteristic flow constant for a particular tube and gas. This constant was evaluated from the data in Fig. 1 by a linear least-squares fit and found to be 2.16×10^{-3} cm^{4}sec/cmHg.

Detector, transducer, and readout system

A flame ionization detector was selected for this study because of its high sensivity, high speed of response, and small sensitive volume. The construction of the detector has been reported elsewhere[11]. The capacitance of the detector and the detector circuit components were measured with an LC meter (Type 130; Tektronix) and the values are given in Table I.

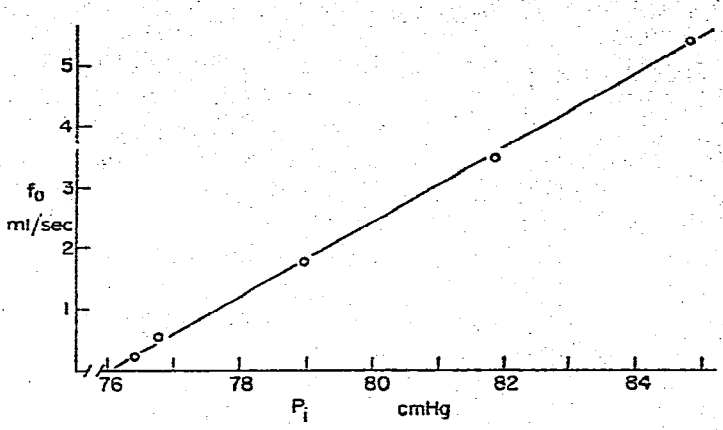

Fig. 1. Flow-rate calibration of the 1-m capillary column.

The operational amplifier electrometer designed for this work is shown in Fig. 2. An amplifier with a gain of two followed the input stage in order to give the 10-V output required for the analog-to-digital converter (ADC). The 51.1 MΩ (0.1%) resistor in the feedback network gave a sensitivity of 9.8×10^{-9} A/V at the input to the ADC. The 120-pF capacitor served to reduce the noise gain at high frequencies and to minimize the overall noise at the output[13]. All connections in the high-impedance circuitry were low-noise coaxial cable (Part No. SC-9; Keithley). In operation, the zero was checked before each injection with an oscilloscope (Model 547, 1A7 plug-in; Tektronix) to within ± 5 mV or ± ½ least significant bit of the ADC. The system grounds, shielding connections, and hum balance were adjusted until the noise and hum levels (peak-to-peak) were below ± 5 mV, as seen at the input of the ADC.

The digital data acquisition and control system was described and illustrated in an earlier publication.[11]

DATA AND COMPUTATION

The experimental data were stored in binary coded octal format in the core memory of a multi-channel pulse-height analyzer (Model 34-27; Nuclear-Chicago). Thus the scope display and Teletype printout were octal representations of the chromatographic peaks and were only qualitatively useful during the course of an experiment as evidenced by the example shown in Fig. 3.

TABLE I

CAPACITANCE OF DETECTOR CIRCUIT COMPONENTS

Component	*Capacitance (pF)*
Detector	6.0
Detector cable	60.6
Shielded battery	35.1
Electrometer cable	95.1

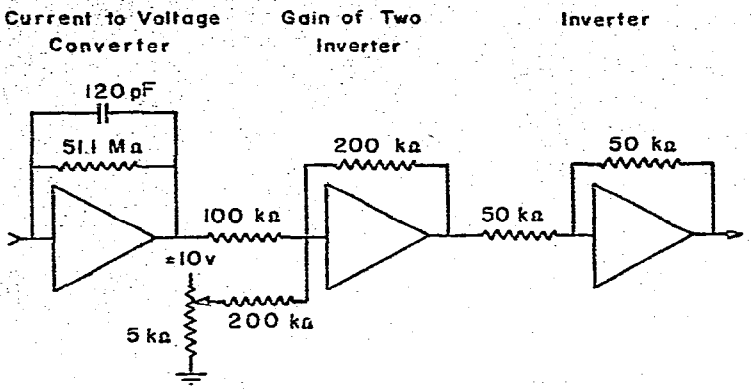

Fig. 2. Operational amplifier electrometer. Amplifiers are Philbrick Type P55AU.

The peak profiles were reduced by a PDP-8/L computer using a program (Moments Analysis for Chromatography; MAC-III) which carried out the octal-to-decimal conversion, and computed the peak area and the normalized first and second moments from the data table stored on paper tape. The source language for the MAC-III program was PAL-III and the calculations were done with the DEC Three Word Floating Point Package (DECUS, No. 08-YQIA-PB). Teletype input/output was provided by the facilities of the floating point package and the Teletype text Input/Output Package (DEC, No. 8-199). The Teletype output of the typical peak profiles are shown in Fig. 4 for valve gate widths from 30 to 100 msec and at various carrier gas flow-rates. The peak areas and first and second moments are tabulated in Table II for the peaks in Fig. 4. It should be noted that 30 msec was found to be the fastest sampling time which could be effected by this valve for quantitative work[11]. At this switching time and at high carrier gas flow-rates, some peak distortion in the form of shoulders may be seen and is explained by the recoil action of the valve. However, this does not seriously effect the calculation of the second moment of the peak. The

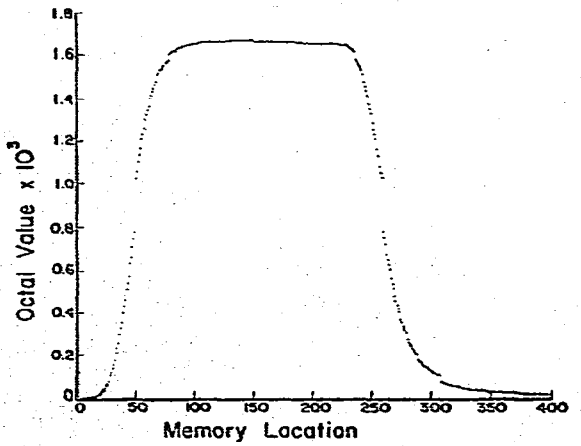

Fig. 3. Binary coded octal output of the experimental data on a decimal display. Valve gate pulse width is 100 msec and the average gas flow-rate is 1.440 ml/sec.

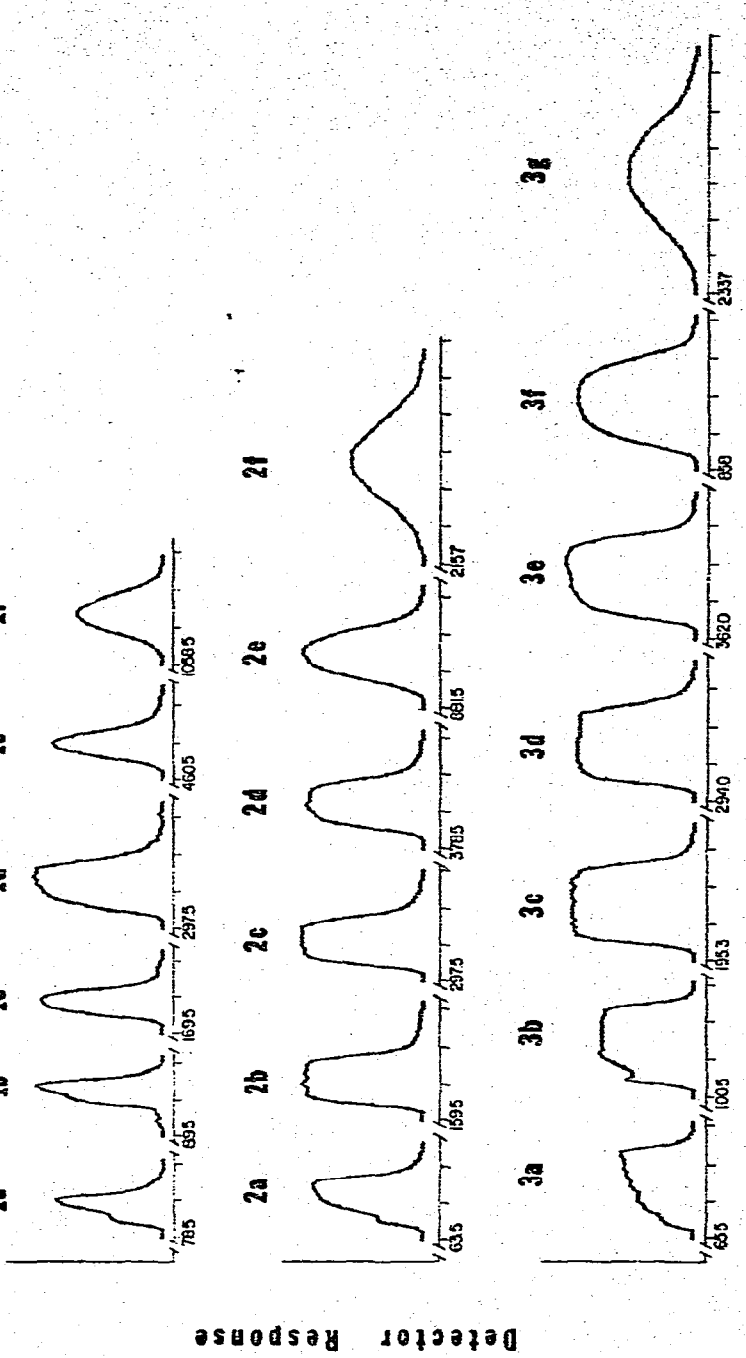

Fig. 4. Printout generated from the moments calculation program. Time-base marks are at 50-msec intervals. Peak profiles are displayed in the order of increasing elution time (see Table II).

TABLE II

DATA FROM THE PEAK AREA AND MOMENT CALCULATIONS AS A FUNCTION OF VALVE GATE WIDTH AND CARRIER GAS FLOW-RATE

Peak no.	*Average carrier gas flow-rate (ml/sec)*	*peak area (V/sec)*	*1st Moment (sec)*	*2nd Moment ($sec^2 \times 10^{-3}$)*
30-msec valve gate				
1a	5.064	0.2966	0.1233	0.2837
1b	3.569	0.3640	0.1527	0.1918
1c	2.361	0.3855	0.2133	0.2298
1d	1.440	0.6975	0.3611	0.5717
1e	0.8640	0.3788	0.5135	0.5262
1f	0.4032	0.4040	1.1281	0.5522
60-msec valve gate				
2a	6.384	0.5028	0.1242	0.4066
2b	2.706	0.6890	0.2184	0.6529
2c	1.440	0.6953	0.3573	0.5992
2d	1.094	0.6481	0.4444	0.6632
2e	0.5184	0.7101	0.9575	0.7284
2f	0.1728	0.7572	2.3075	2.6283
100-msec valve gate				
3a	6.670	0.5151	0.1431	0.9276
3b	3.857	0.7497	0.1800	0.9374
3c	2.073	1.0623	0.2749	1.0924
3d	1.440	1.0284	0.3744	1.1375
3e	1.094	1.1089	0.4553	1.4306
3f	0.5184	1.0606	0.9595	1.3171
3g	0.2304	0.8871	2.5145	3.8385

dependence of the peak profile on the flow-rate is clearly seen from Fig. 4 as is the marked effect of the band-broadening operators at these flow-rates.

The peak areas were calculated from the defining integrals[14] by Simpson's rule

$$I = \frac{h}{3}[y(t_0) + 4y(t_1) + 2y(t_2) + 4y(t_3) + \ldots + 2y(t_{n-2}) + 4y(t_{n-1}) + y(t_n)] \quad (3)$$

where I is the approximate value of the appropriate integral, h is the data logging time interval, and y is the value of $S(t)$. Simpson's rule was chosen for these calculations because of its greater accuracy than the trapezoidal or rectangular rules[15]. The only restriction imposed by the selection of Simpson's rule is that an even number of data points must be used in the computation.

Fig. 5 gives the flow diagram for the section of MOMSIM which computes the value of the integral and concurrently calculates the first and second moments (m_1 and m_2, respectively) by accumulating sums of the first and second powers of time and $f(t)$. At the end of the subroutine, the second moment is adjusted to the center of gravity of the peak by

$$m_{2,0} = m_2 - m_1^2 \quad (4)$$

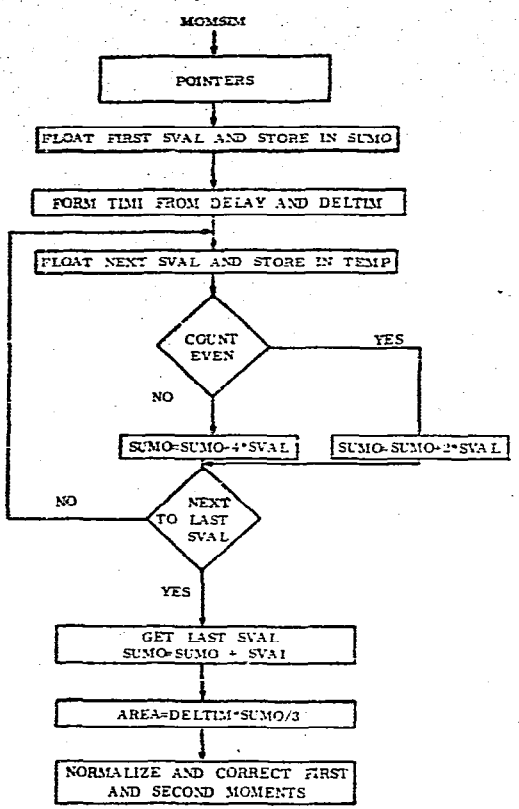

Fig. 5. Flow diagram of the area calculation portion of the MOMSIM subroutine of MAC-III.

RESULTS AND DISCUSSION

Electrical limitations to band broadening

There are two types of limitations on the flame detector response speed:

(1) The rates of the ionization reactions and the transport processes in the effective detector volume;

(2) the electrical time constant of the detector as an RC network. The second contribution will be considered to be the only significant contribution to band broadening. The capacitance of the detector is the capacitance of the collecting electrode with respect to its surroundings. The apparent source resistance may be obtained by considering the current–voltage curve in Fig. 6. The current plateaus represent the current passing through the detector with different amounts of sample. Although a flame detector in saturation is in a non-ohmic region, at a sufficiently small voltage the detector will exhibit ohmic behavior. An apparent source resistance may be defined by the slope of the curves in the ohmic region. The current obtained using the apparent source resistance forms the upper limit on the current which the detector would pass with a given bias voltage, assuming a sufficient concentration of charge carriers. It is this last provision which causes the plateaus; the detector is operated under conditions such that the sample current is less than the limiting ohmic current.

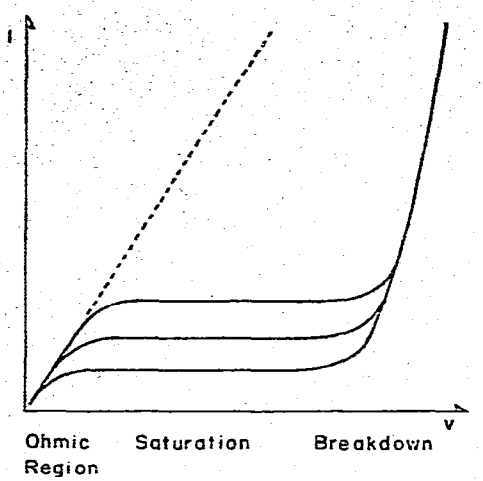

Fig. 6. Characteristic current–voltage curve for the hydrogen flame ionization detector.

The apparent source resistance of the detector was measured using a Keithley Model 601 electrometer in the constant current ohmmeter mode. The maximum potential which can appear across the flame with the Keithley electrometer is 10 V, which is much lower than the voltage required for saturation. Therefore, the resistance obtained was the slope of the current–voltage curve in the ohmic region. With this detector geometry, a helium carrier gas flow-rate of 1 ml/sec and a hydrogen flow-rate of 1 ml/sec, the apparent source resistance was found to be 6.7×10^7 ohms under background conditions. This value with the measured capacitance of the detector (Table I) gives a detector time constant of 0.40 msec.

The time constant of the detector circuit may be calculated by considering the resistance and capacitance of the detector to form part of the input circuit of the operational amplifier as shown in Fig. 7. The analysis requires that the operational amplifier must have a sufficiently large gain bandwidth product so that at the largest frequencies of interest, the amplifier will have a sufficient loop gain to control the summing junction. The other limitation is that the slewing rate of the amplifier must

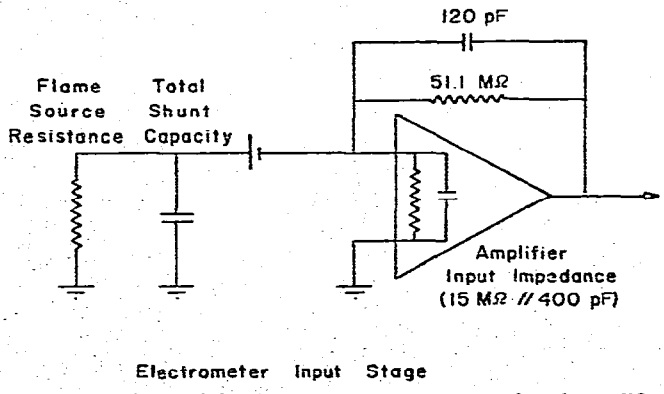

Fig. 7. Analysis of the detector input and operational amplifier electrometer for the calculation of the effective electronic second moment contribution.

be large. The amplifiers used (Philbrick, P55AU) satisfied these requirements (gain bandwidth product 1.5 MHz, slewing rate 1.5 V/sec). Under these conditions, the limitation on the speed of the amplifier circuit is formed entirely by the feedback and the composite input circuits.

The external input circuit is effectively the 6.7×10^7-Ω resistance of the detector shunted by the 197–pF capacitance of the detector, cables, and shielded battery (Table I). This network is shunted by the input impedance of the amplifier (15×10^6 Ω shunted by 400 pF). The resulting time constant is 7.35 msec.

The assumptions involving the amplifier were tested by replacing the detector with a 5.11×10^7-Ω resistor. When the current through the resistor reached its equilibrium value, the current was terminated by disconnecting the resistor from ground. The output of the electrometer was measured from the decay of the current and found to be 8.9 msec. The corresponding value calculated from the known equivalent input circuit parameters is 6.85 msec (for the 51.1-MΩ input resistor). The larger measured time constant is due to the time constant of the feedback network.

The value of the feedback capacitor for unconditional stability was calculated to be 144 pF[13]. In order to maintain maximum bandwidth with a minimum overshoot, the capacitor was reduced to 120 pF giving a feedback network time constant of 6.14 msec. The noise gain and overshoot (*ca.* 1% with a step input) were satisfactory at this level. The total time constant calculated by quadratic addition is 9.2 msec (for the test circuit with the 51.1-MΩ input resistor). This value differs from the measured value (8.9 msec) by only 3.3%. When the time constant of the detector–amplifier circuit is calculated, the total time constant becomes 9.6 msec.

A 10-bit successive approximations converter was used which had an aperture time of 33 μsec. This cannot be considered to be a significant band-broadening contribution in light of the discussion above. We have previously pointed out that even if the signal exceeds the rate limit calculated for the ADC that the data are not broadened by this type of converter[11]. Rather the precision of the amplitude data is decreased, but only during that short period of time where the rate limit is exceeded.

TABLE III

REPRODUCIBILITY OF THE SAMPLING VALVE

Valve gate width = 100 msec; sample = 0.89 μl; methane at STP; F_o = 1.4 ml/sec. The values of retention time and second moment are not corrected for instrumental contributions.

Area ($\times 10^{-9}$ *C*)	*Retention time* (*msec*)	*2nd Moment* (*msec*^{2})
100.5	374.4	1138
99.95	373.8	1133
99.76	374.3	1141
99.66	374.3	1136
99.95	375.1	1131
100.0	374.9	1135
Average		
99.97	374.5	1136
Rel. std. dev.		
0.29%	0.13%	0.31%

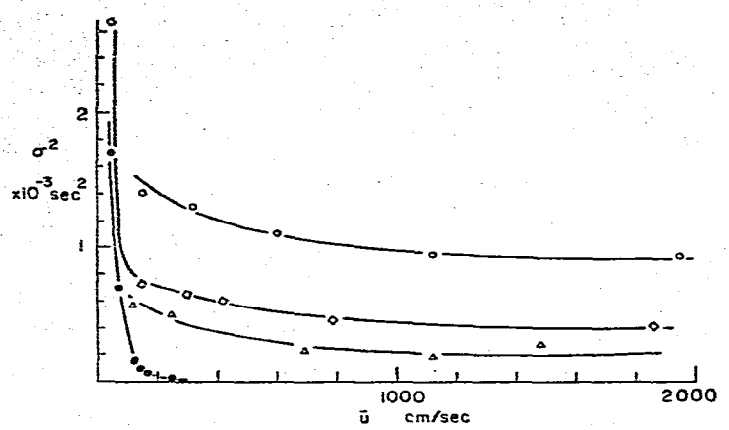

Fig. 8. Variation of the total second moment with the average linear carrier gas velocity. ○ = 100-msec valve gate, ◇ = 60-msec valve gate, △ = 30-msec valve gate; ● = longitudinal diffusion contribution.

Pneumatic band broadening contributions

The excellent reproducibility of the sampling valve is shown in Table III. This also demonstrates the long-term pneumatic stability of the system as the points were taken at 5-min intervals. The significant feature of this valve is the concentration profile resulting from the injection. This was discussed and illustrated in Fig. 12 of ref. 11 and shown to closely approximate a rectangular function. This is essential for the experimental verification of the proposed model[14].

The total experimental second moments for the three different valve gate widths are plotted against the average linear gas velocity in the column in Fig. 8. Also plotted on this figure is the band-broadening contribution due to the radial velocity distribution and longitudinal diffusion. This calculation is based on an inter-diffusion coefficient of 1.005 cm^2/sec for methane in helium at atmospheric pressure[16].

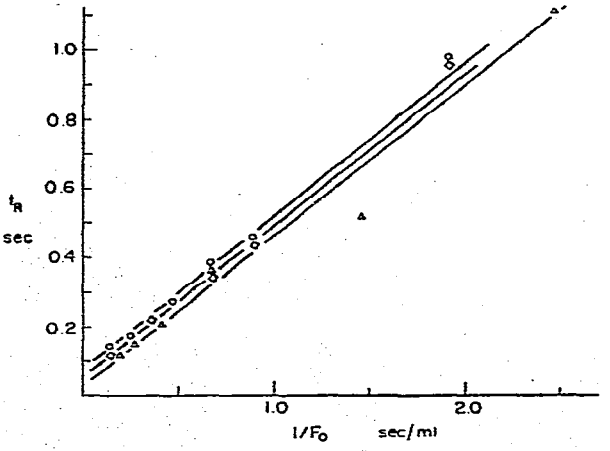

Fig. 9. Variation of retention time with the reciprocal carrier gas flow-rate. ○ = 100-msec valve gate, ◇ = 60-msec valve gate, △ = 30-msec valve gate.

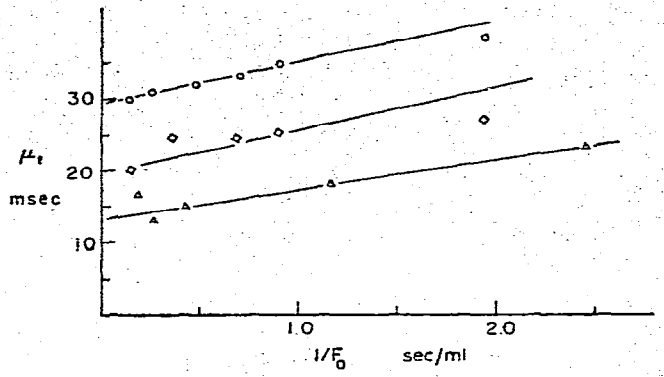

Fig. 10. Variation of the time-based second moment with the reciprocal carrier gas flow-rate. ○ = 100-msec valve gate, ◇ = 60-msec valve gate, △ = 30-msec valve gate.

Comparison of the curve giving the open-tube contribution to the curves giving the total broadening shows that this contribution may be neglected for the conditions of these experiments.

The total experimental second-moment broadening curves approach a limiting straight line at large values of the average carrier gas velocity. These limiting lines are displaced in the order of the valve-gate signal width, or the sample width. The curvature in the line for the 30-msec valve-gate width appears to be due to an experimental artifact or to the magnitude of the experimental error.

The moments calculated from the slopes and intercepts of Figs. 9–11 are tabu-

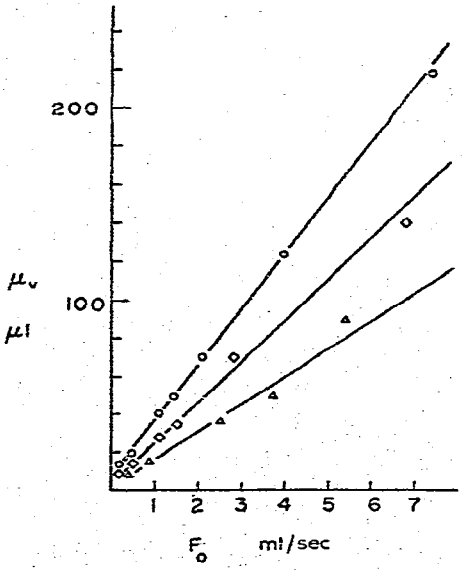

Fig. 11. Variation of the volume-based second moment with the carrier gas flow-rate. ○ = 100-msec valve gate, ◇ = 60-msec valve gate, △ = 30-msec valve gate.

TABLE IV

LEAST SQUARES FIT TO THE MODEL FOR THE FIRST MOMENT CONTRIBUTIONS

m (ml)	*b (msec)*	*Correlation coefficient*	*RMS deviation in t_R (sec)*	*Percent error in slope*
30-msec valve gate				
0.4389	37.70	−0.9990	0.016	−0.88
0.4393	37.77	−0.9990	0.016	−0.89
0.4404	36.86	−0.9990	0.016	−0.90
Average 0.4395	37.44			
60-msec valve gate				
0.3872	104.0	−0.9977	0.051	−1.93
0.3879	103.7	−0.9977	0.051	−1.71
0.3881	103.3	−0.9977	0.051	−1.71
Average 0.3877	103.7			
100-msec valve gate				
0.4614	61.87	−0.9987	0.014	−1.95
0.4626	61.90	−0.9988	0.013	−1.87
0.4633	60.99	−0.9988	0.013	−1.87
Average 0.4624	61.59			

lated in Tables IV–VI. The average value for each data point and the RMS deviation is given to provide a measure of the reproducibility of the data. In the extended calculations, the three replicates were used separately.

A least squares fit for the curves in Figs. 9–11 was done with a program based

TABLE V

LEAST SQUARES FIT TO THE MODEL FOR THE TIME-BASED SECOND MOMENT CONTRIBUTIONS

m′ ($\times 10^{-3}$ ml)	*b′ (msec)*	*Correlation coefficient*	*RMS deviation in μ_t (msec)*	*Percent error in slope*
30-msec valve gate				
3.733	13.36	−0.9935	0.37	−4.6
3.868	13.08	−0.9724	0.81	−10.0
4.180	12.41	−0.9907	0.50	−5.9
Average 3.927	12.95			
60-msec valve gate				
5.185	20.45	−0.9829	1.9	−4.6
5.335	20.46	−0.9794	2.1	−5.2
5.174	20.67	−0.9808	2.0	−4.9
Average 5.231	20.53			
100-msec valve gate				
3.162	30.66	−0.9362	0.70	−12.0
5.218	30.32	−0.9187	1.3	−14.0
4.192	30.86	−0.8497	1.5	−21.0
Average 4.191	30.61			

TABLE VI

LEAST SQUARES FIT TO THE MODEL FOR THE VOLUME-BASED SECOND MOMENT CONTRIBUTIONS

m'' (msec)	*b'' (10^{-3} ml)*	*Correlation coefficient*	*RMS deviation in μ_o (10^{-3} ml)*	*Percent error in slope*
30-msec valve gate				
12.86	4.421	−0.999	0.75	−2.0
12.03	5.366	−0.992	2.0	−5.5
11.77	5.091	−0.997	1.3	−3.5
Average 12.22	4.959			
60-msec valve gate				
19.57	7.071	−0.996	3.9	−2.7
19.76	7.108	−0.996	4.2	−2.9
19.94	6.912	−0.996	4.0	−2.7
Average 19.76	7.030			
100-msec valve gate				
29.78	4.772	−0.9998	1.3	−0.45
29.49	6.547	−0.9997	1.6	−0.81
29.51	6.531	−0.9997	1.6	−0.77
Average 29.59	5.950			

on the Least Squares Subroutine (DECUS, No. 8-134). This subroutine provides the correlation coefficient, the root mean square deviation of the ordinate, and the percent error in the slope in addition to the value of the coefficients of the linear equation. The procedure of obtaining the coefficients from the best straight line through all of the points will give the intercept a slightly different value than it would have had if the data had been fitted to a hyperbola. There will also be slight error introduced in the slope of the line, but due to the close approach of the hyperbolic form to the straight line at the large flow-rates, the values of the physical constants of the model will be obtained from the slope rather than the intercept.

The correlation coefficient provides a measure of the fit to the linear equation. A value near zero indicates that the data does not fit a linear equation while a value of $\pm$ 1 indicates a very good fit[17]. The percent error in the slope is a measure of the range of slopes with which a straight line can be drawn through the points due to the scatter of the data points.

In the case of the least squares fit to the equation derived from the superposition of the first moments for the model[14]

$$t_R = \frac{1}{F_o}\left(\frac{\pi r^2 L}{J} + V_m + \frac{V_d}{2}\right) + \left(\tau_e + \frac{t_g}{2}\right) \tag{5}$$

the slope of the line for each valve gate width in Table IV should be the same (t_R = retention time; r = radius of the tube; J = compressibility factor; V_m = mixing volume; V_d = detector sensitive volume; τ_e = time constant of the detector and associated electronics). Although the values for the slope of the 60-msec valve gate are smaller than the values for the 30- and 100-msec gate widths, this is the

only one which gives a reasonable value for the sum of V_m and $V_d/2$. For the 60-msec gate this sum is 23 μl which should be compared to 75 μl for the 30-msec gate and 98 μl for the 100-msec valve gate width. A similar discrepancy appears in the intercept, except that the 60-msec valve gate value is much larger than the other two values. This value is also much larger than the expected value (9.6 msec + 30 msec). The expected values for the other two valve gate widths are much closer to the experimental values (24.6 msec for the 30-msec gate and 59.6 for a 100-msec gate). This may be explained by the poor resetability of the methane pressure between experiments. The effect of small changes in the sample concentration should be corrected by the normalization of the moments; however, relatively large changes will effect the value of the moments.

From the equation derived for the time-based second moment[14]

$$\mu_t = \frac{1}{F_o}\left(V_m^2 + \frac{V_d^2}{48}\right)^{\frac{1}{2}} + \left(\tau_e^2 + \sigma_s^2\right)^{\frac{1}{2}} \tag{6}$$

it can be seen that the slope of all of the lines should be the same as the quadratic sum of the mixing volume and the detector sensitive volume. The values in Table V are within the experimental error. In this case the correlation coefficients are not quite as large as in Table IV, but are sufficiently large to indicate a linear fit at the 99% confidence level with the exception of one value. The error in the slope is also much larger but it is still a reasonable value except for the 100-msec valve gate data group. Comparison of the intercepts with the observed results in Table VII shows excellent results.

The best values of the quadratic sum of the exponential time constant of the detector and the second moment of the sample should be obtained from the volume-based second moment μ_v for the model[14].

$$\mu_v = F_o\left(\sigma_s^2 + \tau_e^2\right)^{\frac{1}{2}} + \left(V_m^2 + \frac{V_d^2}{48}\right)^{\frac{1}{2}} \tag{7}$$

The values of the slope in Table VI should be compared to the values of the intercepts in Table V and to the independently calculated values in Table VII. The values of the slope from the volume-based second moment tend to be somewhat smaller than the intercept values in Table V. This is to be expected from the discussion of the linearization process, hence the values of the quadratic sum of the detector-electrometer time constants and the sample second moment obtained from the slope of eqn.

TABLE VII

COMPARISON OF SECOND MOMENT CONTRIBUTIONS

Valve gate (msec)	*Slope from μ_v* $(\sigma_s^2 + \tau_e^2)^{\frac{1}{2}}$ (msec)*	*Intercept from μ_t* $(\sigma_s^2 + \tau_e^2)^{\frac{1}{2}}$ (msec)*	*Calculated value (msec)*
30	12.2	13.0	12.9
60	19.8	20.5	19.8
100	29.6	30.6	33.0

* These values are the average values of the three replications.

TABLE VIII

SUMMARY OF INSTRUMENTAL BAND-BROADENING CONTRIBUTIONS

Contribution	*Characteristic value*	*Second moment (msec²)*	*Type of contribution*
Mixing volume* (1 ml/sec)	4.4 μl	19.4	Exponential
Detector, electrometer, and cable time constant**	9.6 msec	92.2	Exponential
Sample	100 msec	834	Rectangular
Open tube	—	*ca.* 0.5	Gaussian

* Average of values from Table IV.
** Calculated for a carrier gas flow-rate of 1 ml/sec.

7 are probably more reliable. This is further supported by the smaller error in the slope given in Table VI. The values of the mixing volumes obtained from the intercepts of eqn. 7 are generally larger than the values found from the slopes of eqn. 6. This is also due to the errors introduced by extrapolation and consequently the more reliable values should be taken from Table V.

The calculated and measured values for the instrumental contributions to band broadening for the experimental system are summarized in Table VIII. These values must be interpreted in the context of the model proposed previously[14]. However, the usefulness of that model in describing a real system is verified by the large value of the correlation coefficients of the least squares fits and the excellent agreement of the experimental values of the sample width and detector-electrometer time constant sum with the independently calculated values. The experimental apparatus was designed to have the general characteristics of a precision, high-speed chromatograph as well as to correspond well to the model. The implications of this are that the methods of obtaining the instrumental contributions of this system could be applied to less specialized apparatus.

REFERENCES

1 R. Kieselbach, *Anal. Chem.*, 33 (1961) 806.
2 R. Kieselbach, *Anal. Chem.*, 35 (1963) 1342.
3 J. H. Knox and L. McLaren, *Anal. Chem.*, 35 (1963) 449.
4 F. A. Vandenheuvel, *Anal. Chem.*, 35 (1963) 1193.
5 G. Guiochon, *Anal. Chem.*, 35 (1963) 399.
6 G. Guiochon, *J. Gas Chromatogr.*, 2 (1964) 139.
7 C. N. Reilley, G. P. Hildebrand and J. W. Ashley, *Anal. Chem.*, 34 (1962) 1198.
8 J. W. Ashley, G. P. Hildebrand and C. N. Reilley, *Anal. Chem.*, 36 (1964) 1369.
9 J. W. Ashley and C. N. Reilley, *Anal. Chem.*, 37 (1965) 626.
10 J. C. Sternberg, *Advan. Chromatogr.*, 2 (1964) 205.
11 T. H. Glenn and S. P. Cram, *J. Chromatogr. Sci.*, 8 (1970) 46.
12 J. C. Sternberg, W. S. Galloway and D. T. L. Jones, in N. Brenner, J. E. Callen and M. D. Weiss (Editors), *Gas Chromatography 1961*, Academic Press, New York, 1962, p. 231.
13 *Application Brief RI*, G. A. Philbrick Researches, Dedham, Mass., 1961.
14 T. H. Glenn and S. P. Cram, *Anal. Chem.*, submitted for publication.
15 D. D. McCracken and W. S. Dorn, *Numerical Methods and Fortran Programming*, Wiley, New York, 1966, p. 172.
16 E. N. Fuller and J. C. Giddings, *J. Gas Chromatogr.*, 3 (1965) 222.
17 H. D. Young, *Statistical Treatment of Experimental Data*, McGraw Hill, New York, 1962.